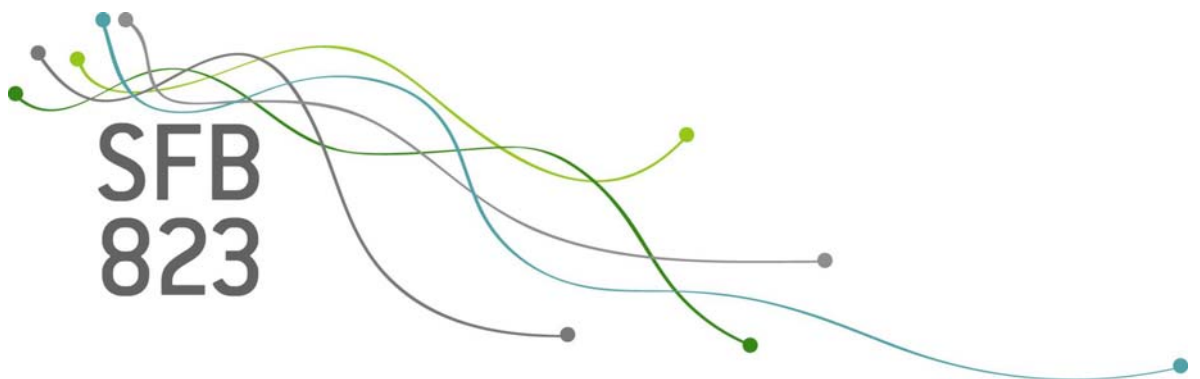# Stochastic modeling and statistical analysis of fatigue tests on prestressed concrete beams under cyclic loadings

Guido Heeke, Simone Hermann, Jens Heinrich, Katja Ickstadt, Reinhard Maurer, Christine H. Müller

Stochastic modeling and statistical analysis of fatigue tests on prestressed concrete beams under cyclic loadings

Guido Heeke[1][*], Simone Hermann[2][†], Jens Heinrich[1], Katja Ickstadt[2], Reinhard Maurer[1], Christine H. Müller[2]

[1] *TU Dortmund University, Faculty of Architecture and Civil Engineering, August-Schmidt-Str. 8, D-44227 Dortmund, Germany*

[2] *TU Dortmund University, Faculty of Statistics, Vogelpothsweg 87, D-44221 Dortmund, Germany*

July 27, 2015

Abstract

To evaluate the fatigue behavior of prestressed concrete, bridges for instance, it is necessary to determine the built in tendons' fatigue strength. Therefore, prestressing steel samples (strands), obtained from an existing bridge built in 1957, were examined and tested by TU Dortmund University, see [1, 2]. Additionally, similar prestressing steels were tested in comparable experiments. As large experiments on prestressed concrete beams under cyclic load with small stress range are very time-consuming and expensive, an early prediction of failure trend in the experiment is desirable. Here, it is shown that a crack width function can be evolved dependent on the process of single wire failures. This process will differ for each experiment because of the randomness of single wire failure. Description of this uncertainty is the first step and is achieved by a predictive distribution for the counting process of wire failure. The second step is to include these results into the model for the crack width process for which a nonlinear regression model based on a physically evolved function depending on the counting process is suitable. For both modeling steps, we present a Bayesian estimation and prediction procedure.

Keywords: Crack growth, fatigue experiments, prestressing steel, long-term tests, counting process, nonlinear regression, Bayesian estimation and prediction.

---

[*]responsible for the engineering part
[†]responsible for the statistical modeling

Nomenclature

u_v	= circumference for transfer of bond stress (mm)
A_p	= surface of prestressing steel (mm^2)
$A_p(n)$	= surface of prestressing steel after n (load) cycles (mm^2)
τ_{bm}	= bond stress (MPa)
f_{ctm}	= mean value of concrete tensile strength (MPa)
ξ	= bond correction factor for post-tensioned strand
σ_{pm0}	= initial tension in prestressing steel (MPa)
$\sigma_{p,max}$	= maximum stress in prestressing steel as result of maximum load (MPa)
$\sigma_{p,min}$	= minimum stress in prestressing steel as result of minimum load (MPa)
$\Delta\sigma_{pr}$	= difference $\sigma_{p,max} - \sigma_{pm0}$ (MPa)
$\Delta\sigma_p$	= stress range, difference $\sigma_{p,max} - \sigma_{p,min}$ (MPa)
l_t	= load influence length (mm)
ε_{cm}	= mean strain of concrete
ε_{pm}	= mean strain of prestressing steel
$\varepsilon_{p,max}$	= maximum strain of prestressing steel as result of load
k_t	= value to consider loading condition and time
E_p	= Young's modulus of prestressing steel (MPa)
n	= applied number of cycles
$w_k(n)$	= crack width after n cycles (mm)
C_n	= number of broken wires after n cycles
m	= total number of wire failures
N_j	= number of cycles up to the jth wire failure, $j = 1, ..., m$
N	= number of cycles at failure time of the concrete beam, i.e. last observation point (usually equal to n_I)
I	= total amount of observations
y_i	= crack width after n_i cycles, $i = 1, ..., I$
$\mathcal{N}(\mu, \sigma^2)$	= normal distribution with mean μ and variance σ^2
$\text{Pois}(\lambda)$	= Poisson distribution with parameter λ
$\Lambda(n)$	= cumulative intensity function of the Poisson process, expected number of broken wires after n cycles
α, β	= parameters of function $\Lambda(n)$
$\widetilde{w}(n, C_n, \theta)$	= crack width function evolved from $w_k(n)$ with parameter θ

1 Introduction

Scientific studies of traffic volume on the German Autobahn uncovered that the current loads exceed the applicable loads based on former traffic load models for calculation of bridges, see [3, 4]. The fact of ongoing traffic growth in Germany can be relayed to many other countries worldwide, for example see [5, 6]. In [7] is described, that Germany has an over-average share in European fright transport, which underlines the especial importance in this case.

There are several approaches to assess the fatigue strength and remaining lifetime of existing prestressed concrete bridges, see, e.g., [8, 9, 10]. To obtain a better understanding of the fatigue behaviour of bridges, it is necessary to study the fatigue behaviour of components of bridges like, for example, cast-in-slabs, precast beams or prestressing steel. Therefore, many studies deal with executed fatigue experiments with prestressed concrete beams ([11, 12, 13, 14, 15, 16, 17, 18]).

In particular, prestressing steel needs to be tested in embedded conditions taking into account friction corrosion, as prestressing steel tested in air possesses higher fatigue strength. For this purpose, various experimental and theoretical research projects have been conducted with post-tensioned concrete beams, see [19, 20, 21]. The aim of these investigations is to provide basics, in the form of S-N curves for post-tensioned steel, in order to make statements on the fatigue strength of prestressed concrete bridges. Having the same aim, prestressing steel samples, obtained from an existing bridge built in 1957, were examined and tested by TU Dortmund University, see [1, 2]. However, cyclic tests of post-tensioned concrete beams are very time-consuming and expensive. Especially at very low stress ranges, which are of particular interest, test time often is several months per test. Therefore, an early prediction of failure is desirable.

Although it is well known that fatigue behaviour is a random process, there are only a few articles using stochastic models and statistical analysis of reliability of bridges as in [22, 23, 24]. A good overview of stochastic models for fatigue behavior is given in [25]. But for data like the ones underlying this paper, it lacks research because such expensive and time-consuming experiments were not done yet. This work fills this gap with a combination of engineering and statistics research. The engineering research provides a functional relationship between the crack width and the amount of broken wires and past load cycles. Statistics research takes this information into a model describing the uncertainties and yields inference that provides a reliable forecast for future observations. Key inputs for that model are a nonhomogeneous Poisson process (NHPP) describing the wire failure process and a nonlinear regression model based on the crack width function characterizing the behavior of the crack width conditional on that wire failure process. For example, [26] employ a NHPP modeling crack initiation in bone cement, [27] adapt a Poisson process to the number of failures of dual-phase steel specimen, and [28] present a Bayesian estimation method for a NHPP and apply it on pitting damage.

The remainder of this work is structured as follows. In the second section, the underlying experiments will be described in detail. The third section contains the development of the function describing the crack width that will be the main object in the fourth section that covers the statistical methods and their application to the data.

2 Experimental procedure

As part of the demolition of an existing prestressed concrete bridge, built in 1957, there was a chance to extract prestressing steel samples. Theses samples were built in 5 test beams (TR01-TR05) to run fatigue tests. 5 strands were embedded in each test beam. Likewise, two further test beams (SB01, SB02) containing strands of new production were prepared and tested up to now. The new strands had similar properties compared to the extracted strands. All prestressing strands used were 7-wire 3/8" strands. Each strand had a diameter of $9.3mm$, a cross-sectional area of $52mm^2$ and a grade St1570/1770. The prestressing steel

was deflected in a shear force free region of the test beam at a length of $2m$ with a minimum radius of $r = 5m$. This considered the influence of fretting corrosion between the tensioned strand and steel duct. The dimensions of the test beams were $4.50m \times 1.00m \times 0.30m$.

Figure 1: Experimental set-up

An essential component of the test beam was a large circular recess in the center. In contrast to a solid cross-section beam, the inner lever arm is almost constant after the test beam changes over in cracked condition. The experimental set-up was designed as a four point bending test. The cyclic loading was realized by a four-column testing machine which can realize a maximum test load of +/-2500kN (Figure 1).

The press force was applied by a spreader bar and two roller bearings into the prestressed concrete beams. The bearing of the beams was almost free of constraint forces by using very stiff swings. At the beginning of each test, an initial crack was induced below the
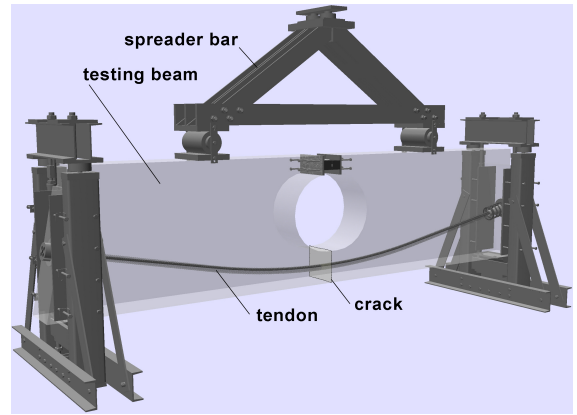

Figure 2: Schematic situation of embedded strand

recess in midspan (Figure 2). After that, the fatigue strength of the embedded prestressing steels was tested under a constant cyclic loading. Testing was performed until a critical number of tension wires failed. The applied stress range $\Delta\sigma_p$, compare Figure 3, in relation to the corresponding fatigue life N denotes the fatigue strength of the tested steel samples embedded in the test beam. For crack width measurement displacement transducers were placed on both sides of the crack at approximately the same level with the tendon. Sudden increase in the periodic measured values serve as a good indicator of broken wires (Figure 3). Due to different crack widths at the beginning of each test ($w_k(n = 0)$) it is senseful to focus only on the growing with start value 0. This leads to the function

$$w_k^0(n) = w_k(n) - w_k(0). \qquad (1)$$

To define exactly the number of load cycles at the failure of a wire, a microphone and an accelerometer were placed at the wedge plate of the stressing anchorage. The microphone recorded the structure-borne noise, the accelerometer the pulse of a wire breakage. Both systems were used redundantly.
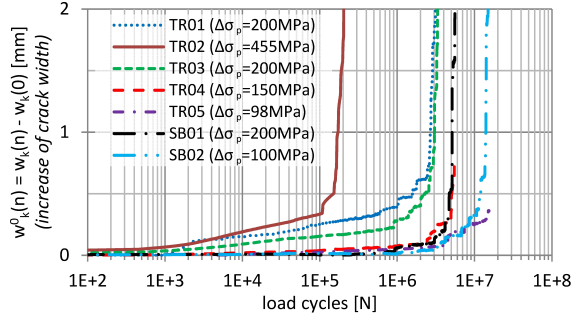
Figure 3: Test results TR01-TR05 and SB01-SB02

3 Mathematical determination of crack width

The damage process of single wire failures can be simulated by calculating the crack width, taking into account the breaking times. This calculation is based on the crack formula for calculating crack widths of a single crack. The test beams have the positive effect that in cracked condition the tension zone only contains prestressing steel and no further reinforcement, which otherwise need to be taken into account for strain determinations in calculations, too. The crack opening w_k corresponds exactly to the difference in expansion between the affected prestressing steel and the surrounding concrete within the load influence length l_t of the crack (Figure 5, subimage 'Strain'). In this area, the tensile stress is transferred from the undisturbed cross section into the prestressed steel. This length includes both sides of the crack. The crack width can now be calculated by determining the mean strain and the load influence length of the crack. In cyclic load tests single wires gradually fatigue over time. In these tests the external load stress is kept constant by the force control of the machine. Thereby the stress increases in the remaining prestressed steel wires with each wire break. In comparison to reinforcing steel the composite properties of prestressing steel are not fundamentally different. Using one tendon, several strands are closely spaced together (Figure 5, subimage 'Cross section'). Therefore, calculations must be done using an equivalent diameter ϕ_p of prestressing steel. According to [24, 29, 30] the

equivalent diameter is given by

$$\phi_p = 1.6 \cdot \sqrt{A_p}$$

for bundles and the circumference for transfer of bond stress by

$$u_v = \phi_p \cdot \pi = 1.6 \cdot \sqrt{A_p} \cdot \pi.$$

By considering a single crack, there is the same strain in the prestressing steel and concrete at the end of the load influence length l_t. Assuming a constant bond stress, the additional stress in the prestressing steel must be initiated across the influence load length to the undisturbed area, in order to establish the following equilibrium condition

$$\Delta\sigma_{pr} \cdot A_p = \xi \cdot \tau_{bm} \cdot l_t \cdot u_v. \tag{2}$$

$\Delta\sigma_{pr}$ is the difference between the maximum prestressing steel stress $\sigma_{p,max}$ in the crack as a result of load and the initial tension σ_{pm0} in the prestressing steel ($\Delta\sigma_{pr} = \sigma_{p,max} - \sigma_{pm0}$), see Figure 4.
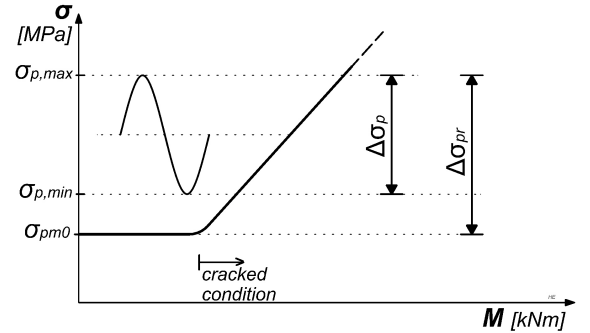

Figure 4: Graphical definition of stress range $\Delta\sigma_p$ and $\Delta\sigma_{pr}$

The complex composite behavior is determined by a variety of influences. Hence, there is no universal bonding rule covering all constraints equally well. Experimental evaluations of other reports indicate that the bond stress τ_{bm} may assumed to be 1.8-times the mean value of the tensile strength of concrete f_{ctm} (simplification).

Because the normative bond stress value τ_{bm} refers to the composite properties of reinforcing steel, it must be adjusted with a correction factor $\xi = 0.5$ for post-tensioned strands

[29]. If these approaches and the effective composite scale are taken into account, it follows by converting and substituting from equation (2)

$$l_t = \frac{\Delta\sigma_{pr} \cdot A_p}{1.44 \cdot \pi \cdot f_{ctm} \cdot \sqrt{A_p}}. \tag{3}$$

In accordance with [29, 30] the integration length of a single crack results from the double value of the load influence length (Figure 5, subimage 'Strain')

$$w_k = 2 \cdot l_t \cdot (\varepsilon_{pm} - \varepsilon_{cm}). \tag{4}$$

Neglecting the concrete strain ($\varepsilon_c = 0$), it follows for the differential strain

$$\varepsilon_{pm} - \varepsilon_{cm} = (1 - k_t) \cdot \Delta\varepsilon_{pr},$$
$$\varepsilon_{pm} - \varepsilon_{cm} = (1 - k_t) \cdot \frac{\Delta\sigma_{pr}}{E_p}. \tag{5}$$

Among others, loading conditions and time have an influence on the bond strength. This effect is taken into account by the value k_t. As experimental tests in other reports showed, the value for short-time loads is recognized as a good approximation to $k_t = 0.6$. A cyclic or long-time load decreases the bond strength significantly. It comes to bond creep between prestressing steel and concrete and consequently to an increase in crack width. This creep effect decreases over time and is reduced during long or cyclic loading to $k_t = 0.4$. This represents about 70% of the applicable value for short-time loads. Thus, value k_t depends on the number of load cycles and can be described easily over time by an exponential function

$$k_t(n) = k_{t\to\infty} + (k_{t=0} - k_{t\to\infty}) \cdot e^{n \cdot c}. \tag{6}$$

At first the function k_t starts with the value of a short-time load ($k_{t=0}$) and approaches later to the value for a long-time load ($k_{t\to\infty}$). The parameter c controls the speed of this composite loss. It was found that in these experiments the value of $c = -2 \cdot 10^{-5}$ generally provides good results. With each wire rupture the cross-sectional area A_p of the prestressing steel will be reduced. Because the stress difference $\Delta\sigma_{pr}$ is directly related to the cross-sectional area A_p,
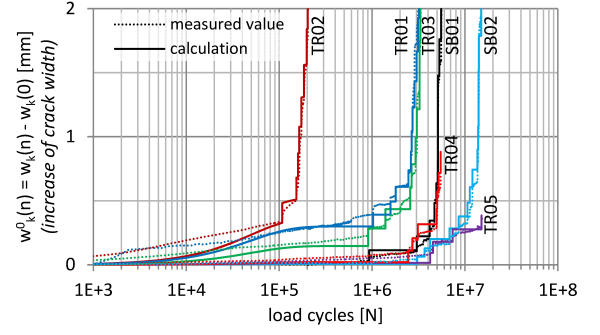

Figure 6: Calculated crack width in comparison to measured values

it is possible to describe $\Delta\sigma_{pr}$ for any number of cyclic loads n by

$$\Delta\sigma_{pr}(n) = \sigma_{p,max} \cdot \frac{A_p}{A_p(n)} - \sigma_{pm0}$$
$$= \sigma_{p,max} \cdot \frac{1}{1 - \frac{C_n}{35}} - \sigma_{pm0}$$

with $A_p(n)$ representing the residual cross-sectional area A_p after n load cycles, i.e. $A_p \cdot \left(1 - \frac{C_n}{35}\right)$, and C_n being the number of broken wires after n load cycles. Taking into account temporal effects, equation (3) and (5) can be inserted into equation (4) resulting in the time-dependent crack width function

$$w_k(n) = \frac{(1 - k_t(n)) \cdot (\Delta\sigma_{pr}(n))^2 \cdot A_p(n)}{0.72 \cdot \pi \cdot f_{ctm} \cdot E_p \cdot \sqrt{A_p(n)}} \tag{7}$$

with $k_t(n)$ the function in (6).

Based on equation (7) and material input parameters the measured crack width can be calculated and displayed as can be seen in Figure 6.

As can easily be imagined, these experiments depend on stochastic error. This uncertainty can be described by a stochastic model.

4 Statistical theory and application

The first important step is to model the wire failure process which by construction is a counting process. When resorting to the most widely used one, i.e. the Poisson process, it is clear
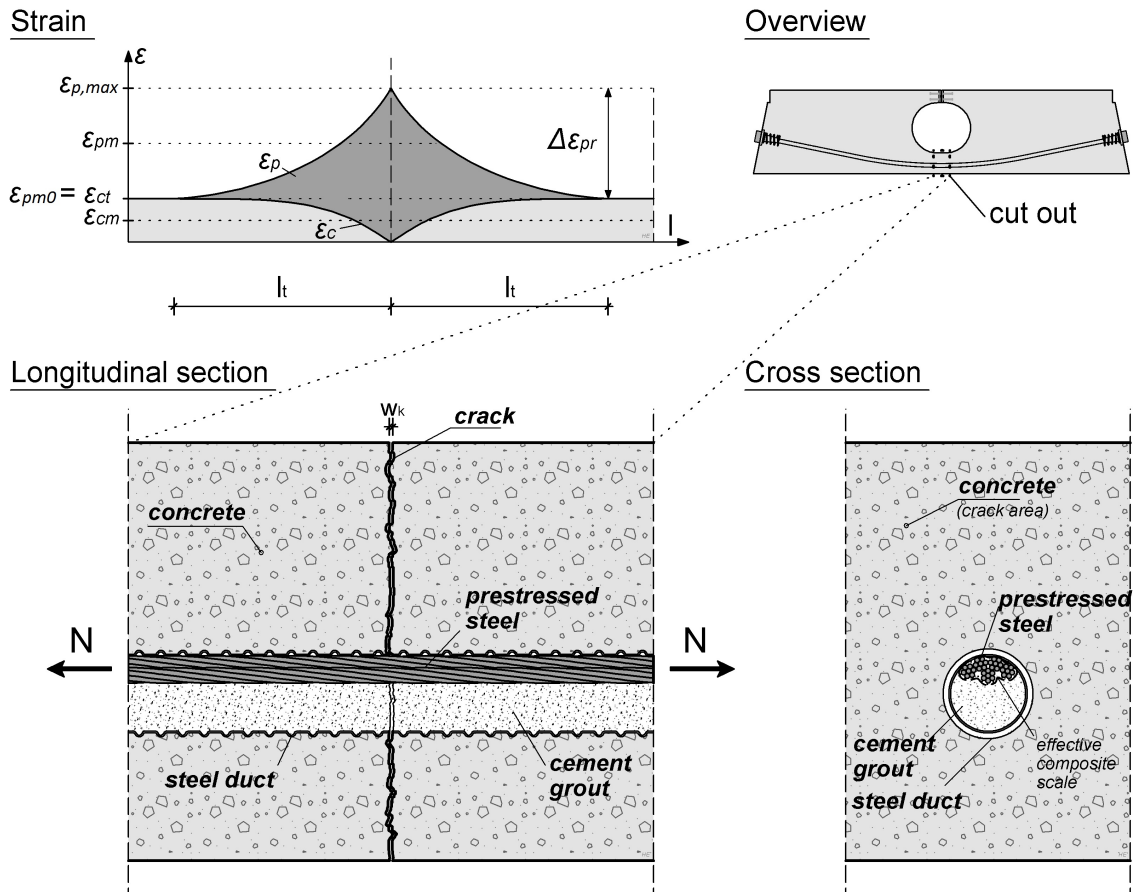
Figure 5: Strain and load influence length of crack in midspan

that a nonhomogeneous specification should be used. When a wire fails, the load distributes on fewer wires and, therefore, the probability that another wire fails grows. Denoting the number of broken wires after n load cycles with C_n we assume the process to start in 0, for arbitrary $0 \leq n_1 < ... < n_I$ the increments $C_{n_2} - C_{n_1}, ..., C_{n_I} - C_{n_{I-1}}$ are assumed to be independent. $C_n - C_l$ is Poisson distributed with parameter $\int_n^l \lambda(u)\, du$ for all $0 \leq n < l$, which leads to a nonhomogeneous Poisson process $\{C_n,\ n \in [0, \infty)\}$ with intensity rate $\lambda(n)$. A good overview of a Bayesian analysis for such a process can be found in [31] whereas [32] display Bayesian estimation for the case of the power law process used in the following. Mathematically, n is a natural number and a Poisson process is a time-continuous process by construction. For our calculations we will divide the number of load cycles by one million to obtain numbers that are easier to handle and have lower risk of rounding errors. Here, we will assume the power law for the expected number $\mathbb{E}[C_n]$ of broken wires after n load cycles as

$$\mathbb{E}[C_n] = \int_0^n \lambda(u)\, du = \Lambda(n) = \left(\frac{n}{\beta}\right)^\alpha,$$

which is also used in [27] and [28]. Λ is called cumulative intensity rate. Its derivative is the hazard rate of the Weibull distribution. The homogeneous case is nested by setting $\alpha = 1$, but here we expect α to be greater than 1 which leads to a growth higher than linear. Obviously we assume $\beta > 0$.

Based on the so called event times $0 < N_1 < ... < N_m < N$ given by

$$N_j = \min\{l:\ C_l = j\},\ j = 1, ..., m,$$

the likelihood is given by

$$p(N_1, ..., N_m|\ \alpha, \beta) = \exp(-\Lambda(N)) \prod_{j=1}^m \lambda(N_j),$$

see [31], p. 119. Here, the information, that after N_m up to the last observed load cycle N no wire fails, slips in.

In Bayesian estimation, the parameters are assumed to be random variables with unknown distribution that needs to be estimated. If one has prior knowledge, maybe from other experiments or because of physical knowledge from experts, one can take that into account using a so-called prior distribution. Since we do not have any specific prior knowledge for the parameters α and β, we use a so-called noninformative approach, where all parameters have the same probability. That means, up to a normalization constant, the likelihood becomes the posterior of the parameters

$$p(\alpha, \beta|\ N_1, ..., N_m) \propto p(N_1, ..., N_m|\ \alpha, \beta),$$

where $\propto$ means 'proportional to', i.e. we drop the constant $\left(\int p(N_1, ..., N_m|\ \alpha, \beta)\, d(\alpha, \beta)\right)^{-1}$ because it is not analytically calculable and, therefore, unknown. The shape of the posterior distribution is given by the likelihood and this fact is used in a sampling method. Here, we employ the widely used Metropolis-Hastings (MH) algorithm, see [33] p. 130. In Figure 7 we see boxplots for the drawn samples for α and β for the seven experiments, which give a good overview of the location and the variance of the approximated posterior distributions. Experiments 1-5 denote TR01-5 and numbers 6 and 7 belong to SB01 and SB02. As mentioned before, for the calculations we take n as the load cycles in millions. The posterior distributions each are approximated with $K = 2000$ samples. This will be the same in all following evaluations.

Based on the MH-resulting samples

$$(\alpha_1^*, \beta_1^*), ..., (\alpha_K^*, \beta_K^*) \sim p(\alpha, \beta|\ N_1, ..., N_m)$$

a predictive distribution can be approximated. We are interested in the development of the process up to a fixed number of n_f load cycles, i.e. in the forecast for a future experiment under equal test conditions. Because the process is uniquely defined by the event times, we will sample $N_1^* < N_2^* < ...$ iteratively. The density of the first event time is

$$p(N_1^*|\ N_1, ..., N_m)$$
$$= \int p(N_1^*|\ \alpha, \beta) \cdot p(\alpha, \beta|\ N_1, ..., N_m)\, d(\alpha, \beta)$$
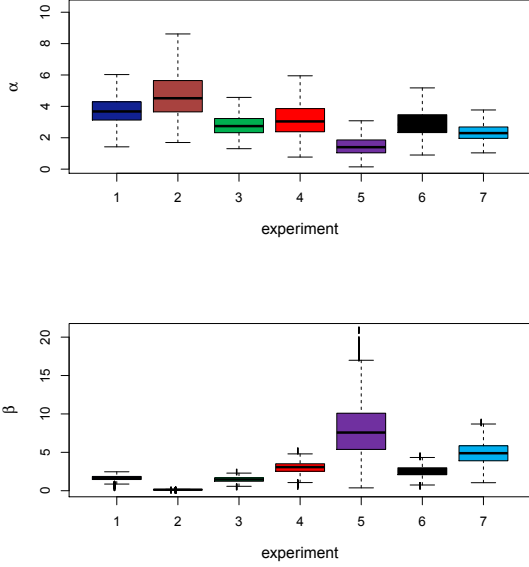$$\approx \frac{1}{K} \sum_{k=1}^K p(N_1^*|\ N_m, \alpha_k^*, \beta_k^*),$$

Figure 7: Boxplots of the posterior distributions of α and β for the seven experiments

Figure 8: Prediction of the wire failure process, for the first experiment (top) and for the six other experiments on a logarithmic scale (bottom)

where $p(N_1^*|\ \alpha, \beta)$ is the density of the exponential distribution with parameter $\Lambda(N_1^*)$. Afterwards, we iteratively sample

$$N_j^* \sim \frac{1}{K} \sum_{k=1}^{K} p(N_j^*|\ N_{j-1}^*, \alpha_k^*, \beta_k^*), \quad (8)$$

$j = 2, 3, \dots$ with

$$p(N_j^*|\ N_{j-1}^*, \alpha, \beta)$$
$$= \lambda(N_j^*) \exp(-\{\Lambda(N_j^*) - \Lambda(N_{j-1}^*)\}).$$

The number of event times differs for each trajectory, because the number of jumps C_{n_f} is random and varies for each path. The sampled event times yield samples of the counting process through

$$C_n^{*(k)} = \{j:\ N_j^{*(k)} \leq n < N_{j+1}^{*(k)}\}, \quad (9)$$

where $N_j^{*(k)}$ is the jth iteratively drawn event time according to (8), $k = 1, \dots, K$. The resulting prediction for the counting process for the seven experiments can be seen in Figure 8. In the upper picture, the process of the first experiment and its prediction is shown. The solid line denotes the true observed process of broken tension wires. The inner dotted line is
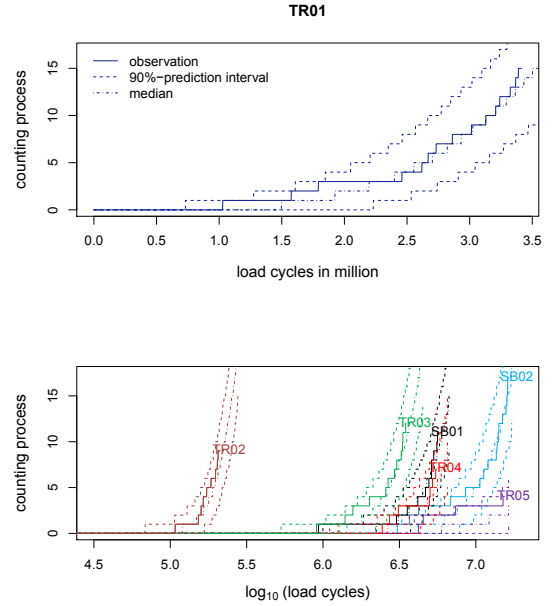
the pointwise median of the processes drawn from the predictive and can be seen as a point prediction. The outer dotted lines are the 0.05- and the 0.95-quantiles which yield a 90% prediction interval. In the lower picture, the six other processes are shown where the x-axis is transformed to $\log_{10}$(load cycles) for a better overview. Except for the fifth series TR05, the median curves mostly follow the true processes and the prediction intervals cover them in all cases except for small parts in the beginning of SB01 and SB02. In the special case of TR05, only four wire failures have been observed until the experiment was stopped because several month had passed. No increasing frequency can be seen for these four points. Therefore, it is not suprising, that our model has difficulties in estimation and prediction for TR05.

In the following we describe the crack width dependent on the counting process. The first step is to transform the function in (1) to a more flexible parametric function with estimable parameters, because some of the constants in that

9

function are approximate values. We obtain

$$\widetilde{w}(n, C_n, \theta)$$
$$= (\theta_1 - \theta_2 \cdot \exp(-n \cdot \theta_3)) \cdot \frac{1}{\sqrt{h(C_n)}} \left(h(C_n) - \theta_4\right)^2$$
$$- (\theta_1 - \theta_2)(1 - \theta_4)^2,$$

where $\theta_1 = \frac{(1 - k_{t \to \infty}) \cdot \sqrt{A_p} \cdot \sigma_{p,max}^2}{0{,}72 \cdot \pi \cdot f_{ctm} \cdot E_p}$, $\theta_2 = \frac{(k_{t=0} - k_{t \to \infty}) \cdot \sqrt{A_p} \cdot \sigma_{p,max}^2}{0{,}72 \cdot \pi \cdot f_{ctm} \cdot E_p}$, $\theta_3 = -c$, $\theta_4 = \frac{\sigma_{pm0}}{\sigma_{p,max}}$ and $h(C_n) = \frac{1}{1 - \frac{C_n}{35}}$.

The corresponding calculation can be found in the appendix. Of course, other parametrizations are possible. However, if more than four parameters are chosen, they will not be identifiable.

The experiments have measurement errors which can be taken into account by our model additevely as follows

$$y_i = \widetilde{w}(n_i, C_{n_i}, \theta) + \epsilon_i,$$
$$\epsilon_i \sim \mathcal{N}(0, \sigma^2),$$
$$C_{n_i} \sim \text{Pois}(\Lambda(n_i)), \ i = 1, ..., I.$$

Here, ϵ_i and C_{n_i} have to be stochastically independent. Conditional on the counting process C_{n_i}, we have a regression model whose parameters can be estimated based on the likelihood. Bayesian inference for nonlinear regression models can be found in [33]. Following from

$$y_i | \ C_{n_i} \sim \mathcal{N}\left(\widetilde{w}(n_i, C_{n_i}, \theta), \sigma^2\right),$$

$i = 1, ..., I$, the conditional likelihood is a product of normal distribution densities. Because of the nonlinear function we have no closed form of the posterior. Therefore, similar to the estimation of α and β, we use a MH-algorithm for the estimation of the parameters with the difference that we can use the physically given constants for an informative Bayesian approach here. That leads to the posterior

$$p(\theta | \ y_1, ..., y_I, \sigma^2) \propto p(y_1, ..., y_I | \ \theta, \sigma^2) \cdot p(\theta),$$

where $p(\theta)$ is the prior density. If we denote with θ^0 the vector resulting from the physical constants given by an expert, we assume $\theta_i \sim \mathcal{N}(\theta_i^0, \theta_i^0)$, $i = 1, ..., 4$, as prior distribution. The variance is chosen equal to the

expected value, which represents a good compromise between the expert knowledge and the large amount of data present. For the error variance σ^2 we choose the inverse Gamma distribution $IG(a, b)$ because then the conditional posterior is an inverse Gamma as well, with parameters $a + \frac{I}{2}$ and $b + \frac{1}{2} \sum_{i=1}^{I} (y_i - \widetilde{w}(n_i, C_{n_i}, \theta))^2$, see [33], p. 35. In our calculations we use $a = b = 1$. The joint posterior of θ and σ^2 can be approximated by drawing using a Metropolis-within-Gibbs sampler, see [33] p. 141. Figure 9 shows boxplots of the posterior distributions for the seven experiments. The black points denote the starting, resp. prior, values. In most cases, they differ from the estimated values. Of course one could pull the posterior in the direction of the initial values with a smaller prior variance, but the estimated variance would become higher.

With the samples $\theta_1^*, \sigma_1^{*2}, ..., \theta_K^*, \sigma_K^{*2}$ from the posterior distribution we can approximate the predictive distribution

$$p(y_i^* | \ y_1, ..., y_I, C_{n_1}, ..., C_{n_I}) \qquad (10)$$
$$= \int p(y_i^* | \ \theta, \sigma^2, C_{n_i}^*) \cdot p(\theta, \sigma^2 | \ y_1, ..., y_I)$$
$$\cdot p(C_{n_i}^* | \ C_{n_1}, ..., C_{n_I}) \, d(\theta, \sigma^2, C_{n_i}^*)$$
$$\approx \frac{1}{K} \sum_{k=1}^{K} p(y_i^* | \ \theta_k^*, \sigma_k^{*2}, C_{n_i}^{*(k)})$$
$$\approx \frac{1}{K} \sum_{k=1}^{K} \frac{1}{\sigma_k^*} \phi\left(\frac{y_i^* - \widetilde{w}(n_i^*, C_{n_i}^{*(k)}, \theta_k^*)}{\sigma_k^*}\right),$$

$i = 1, ..., I$, where ϕ denotes the density of the standard normal distribution. $C_{n_i}^{*(k)}$, $k = 1, ..., K$ are the samples from the predictive distribution of the Poisson process defined in (9).

The distribution in (10) can be approximated with rejection sampling, see [33], p. 116, where one has to choose a candidate area. Here, the interval $[-0.5, y_I + 5]$ is taken with a grid of 0.002. In Figure 10 we see the pointwise prediction results for the seven experiments. In all cases, the 90% prediction intervals cover the true process. Similar to Figure 8 the solid line is the true process, the inner dotted line the mean and the outer dotted lines the 5% and 95% quantiles of the predictive distribution. In the cases of TR01, TR03, TR04 and TR05, the
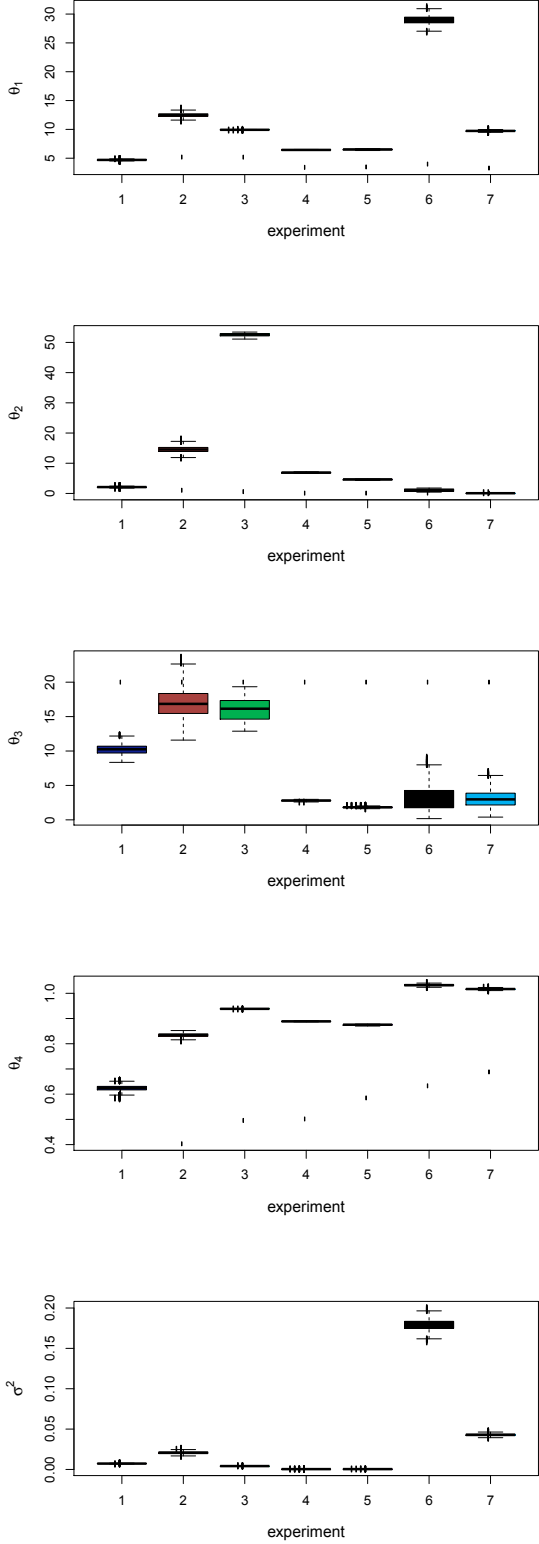
Figure 9: Boxplots of the posterior distribution of $\theta = (\theta_1, \theta_2, \theta_3, \theta_4)$ and σ^2, the black points mark the starting, resp. prior, values given by an expert

mean curve follows the true processes very well. In the other cases – TR02, SB01 and SB02 – the last two or three true jump heights are bigger than predicted. This result is not suprising, because we fit a parametric function to the data. Estimation yields the parameters that fit the data with minimal variance under the assumption of normal distributed errors. The last few observations do not carry much weight in this procedure.
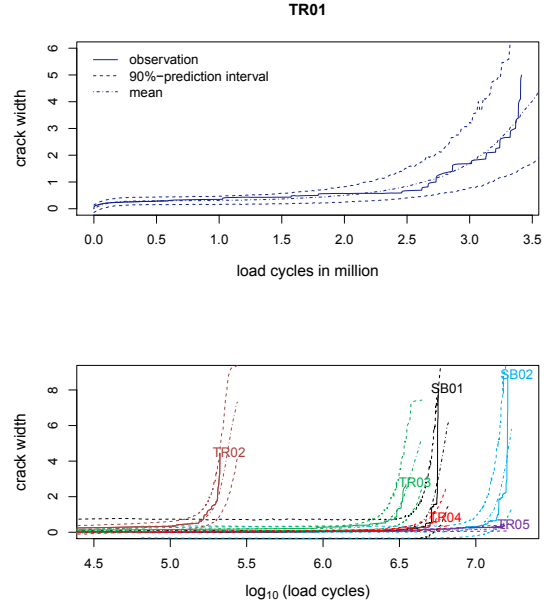

Figure 10: Prediction of the crack width, for the first experiment (top) and for the six other experiments on a logarithmic scale (bottom)

Next, we take a look at the function $\widetilde{w}$ and especially the role of θ_2 and θ_3. Figure 11 shows that this part of the function only describes the very beginning of the series and stays constant for the rest, except for the second experiment. However, we are mainly interested in the prediction for the last part of the experiment and we lose efficiency by estimating needless parameters.

Therefore, we simplify the function $\widetilde{w}$ to

$$\widetilde{w}_s(C_n, \theta) = \widetilde{\theta}_1 \cdot \frac{1}{\sqrt{h(C_n)}} \left(h(C_n) - \widetilde{\theta}_4 \right)^2$$

and estimate the parameters similar to the regression model defined above, but noninformative, because the prior knowledge is lost with
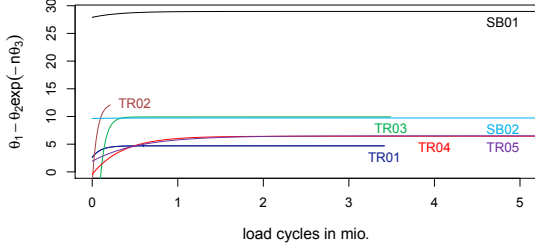
Figure 11: $\widehat{\theta}_1 - \widehat{\theta}_2 \cdot \exp(-n \cdot \widehat{\theta}_3)$, with $\widehat{\theta}_i$ each the mean of their posteriors, $i = 1, 2, 3$

the transformation. This does not pose a problem as the estimations of the parameters differed from the prior values, confer Figure 9. The resulting predictions can be seen in Figure 12. The only difference to the predictions shown in Figure 10 is the beginning of the curve. Therefore, this simplified curve is taken for the prediction of the future development.
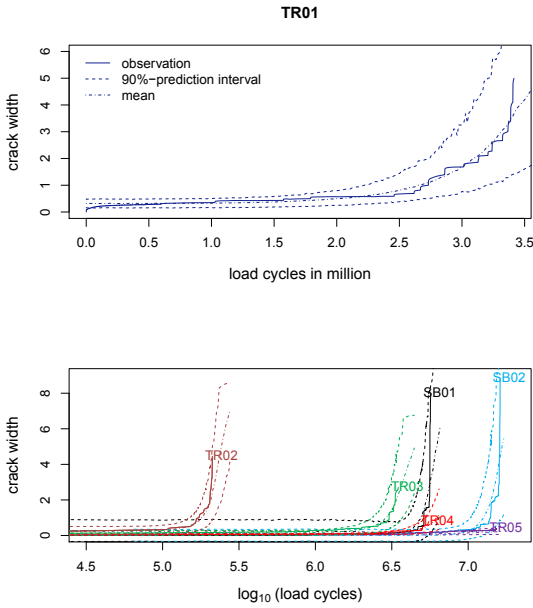

Figure 12: Prediction of the crack width with the simplified curve $\widetilde{w}_s$, for the first experiment (above) and for the six other experiments on a logarithmic scale (bottom)

The last open question is what happens, if we observe the process up to n_I load cycles and are interested in some prediction for a point n_f

with $n_f > n_I$. To that end, we truncate the existing series and compare the predictions with the observed points. For the five experiments TR01-TR05, we take 80%, for SB01 95% and for SB02 90% of the observations for the estimation. In Figure 13 we can compare the posterior distributions with the whole series ('all') and the posterior with the truncated series ('first'). Except for the second experiment TR02 and the sixth experiment SB01, all α have a lower location when using the truncated series, which leads to a lower increasing frequency of the jump process. It seems to be a good idea to use an informative Bayesian estimation approach for the prediction of the unobserved future process. But until now, all experiments are made under different conditions, which leads to very different parameters. How knowledge of these experiments can be used for following ones under new experiment conditions is the subject of future work.
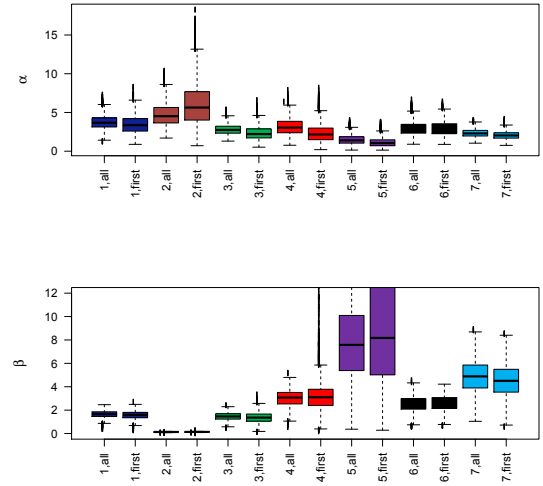

Figure 13: Comparison of the estimations of α and β, each left for the whole series, right for the truncated series

For the counting process we now accordingly sample from

$$N_{m+i}^* \sim \frac{1}{K} \sum_{k=1}^{K} p(N_{m+i} \mid N_{m+i-1}^*, \alpha_k^*, \beta_k^*)$$

$i = 1, 2, ...$ and starting value $N_m^* = N_m$. In Figure 14 we see the predictions for the counting

process. The first impression of the parameter posteriors is supported. Firstly, we can say that in all cases except the seventh jump in TR04, the prediction intervals cover the true process. Secondly, in all cases the point prediction, i.e. the pointwise median, lies a bit below the true process. But considering the challenge predicting such a process with that few observations without using prior knowledge poses, this result is suprisingly good.
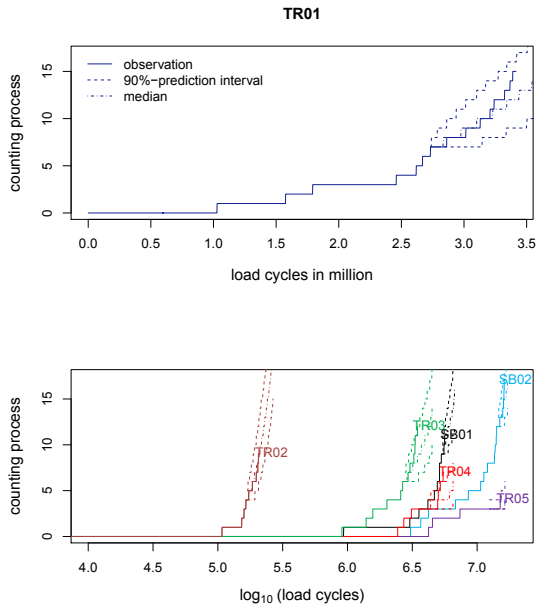

Figure 14: Prediction of the wire failure process for $n_f > n_I$, for the first experiment (top) and for the six other experiments on a logarithmic scale (bottom)

In Figure 15 we compare the posterior distributions of the parameters in $\widetilde{w}_s$ and the corresponding error variance of the regression model, each for the estimation using the whole and the truncated series. In all cases the estimated variance is smaller for the estimations based on the truncated series. As mentioned before, the estimation of the parameter does not take into account whether some points at the end of the series are not well fitted, if the variance averaged over all observations is small. If we truncate just the last nonfitted points, the estimated variance gets smaller. For the curve parameters, only for the third experiment TR03

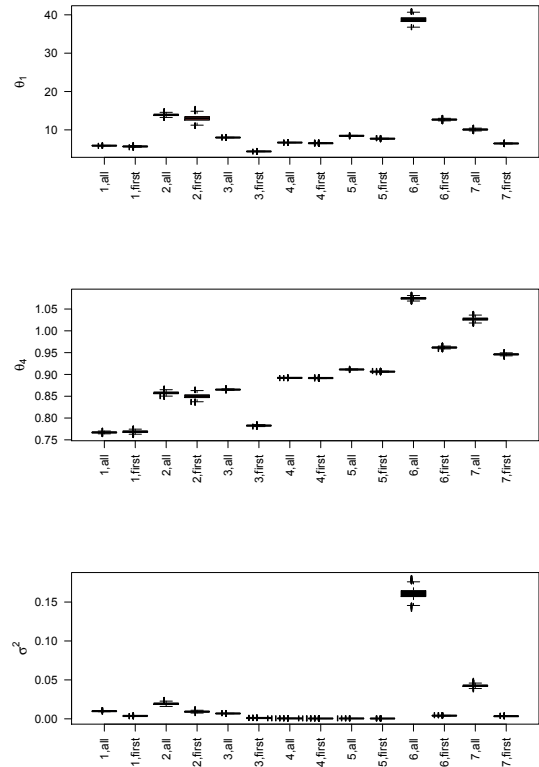and the last two SB01 and SB02, the posteriors differ considerably.

Figure 15: Comparison of the estimations of $\widetilde{\theta}_1$, $\widetilde{\theta}_4$ and σ^2, i.e. the parameters of the regression model with the simplified curve $\widetilde{w}_s$, each left for the whole series, right for the truncated series

The theroetical predictive distribution for the crack width in this prediction procedure stays the same as before, confer (10). In Figure 16 we see the predictions for the crack width curve, which mainly depend on the prediction of the wire failure process shown in Figure 14. The parameters of the regression function can vary to a certain extent, but the prediction result for the crack width closely follows the result for the counting process.

5   Conclusions

A stochastic model has been developed to describe and predict the fatigue process of prestressed concrete beams. In this paper, a func-
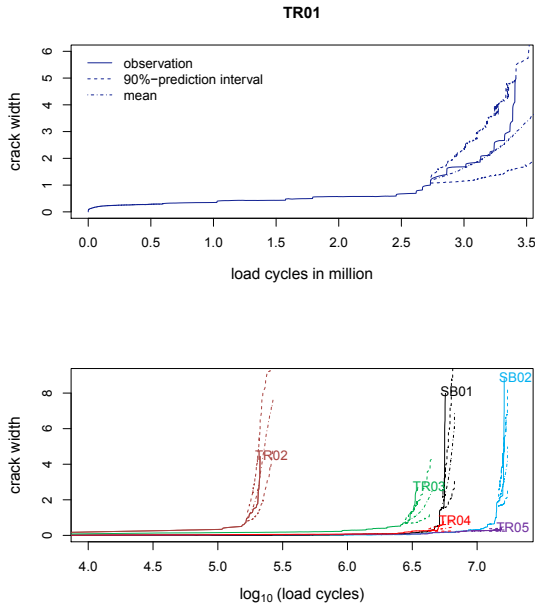
Figure 16: Prediction of the crack width for $n_f > n_I$, for the first experiment (top) and for the six other experiments on a logarithmic scale (bottom)

tion with physical and mechanical background has been developed. This function describes the relation between number of load cycles, number of broken wires in prestressed strands and crack width in the concrete.

Furthermore, inference and prediction for a regression model including a Poisson process has been proposed for this problem. In a first step, a nonhomogeneous Poisson process with the Weibull hazard rate as intensity function has been applied to the wire failure process. It turned out that this process can be fitted reliably by the presented approach. For the prediction of the future development based on a first part of the experiment, prior knowledge should be included. It will be future work, how to use information of existing experiments under different conditions for reliable prior distributions.

Depending on the counting process, a non-linear regression model based on the evolved crack width curve has been applied to the seven expriments. Here, we also predicted the crack width. It turned out that the prediction of

the crack width curve mainly depends on the prediction of the wire failure process. If this prediction works well, the predictions of the crack width in turn are reliable.

Acknowledgements

References

[1] Maurer, R., and Heeke, G. (2010). Ermüdungsfestigkeit der Spannstähle einer Autobahnbrücke von 1957 im einbetonierten Zustand, Abschlussbericht Forschungsvorhaben Straßen.NRW. (FE No. 00 08 5001)

[2] Maurer, R., Heeke, G., and Marzahn, G. (2012). Fatigue strength of prestressing steel tendons embedded in concrete of an aged highway bridge/Ermüdungsfestigkeit der Spannstähle einer Autobahnbrücke von 1957 im einbetonierten Zustand. *Bauingenieur* **87** (5), 226–236.

[3] Kaschner, R., et al. (2009). Auswirkungen des Schwerlastverkehrs auf die Brücken der Bundesfernstraßen. Berichte der Bundesanstalt für Straßenwesen, Brücken- und Ingenieurbau. Heft B 68, Bergisch Gladbach.

[4] Naumann, J. (2010). Bridges and heavy goods traffic - an inventory/Brücken und Schwerverkehr - eine Bestandsaufnahme. *Bauingenieur* **85** (1), 1–9.

[5] International Road Federation (2009). *IRF World Road Statistics*, Geneva.

[6] Department for Transport (2011). *Annual Road Traffic Estimates*. Road Traffic Statistics, London.

[7] European Commission (2012). EU transport in figures. *Statistical Pocketbook.* Publications Office of European Union, Luxembourg.

[8] Al-Zaid, R. Z., and Nowak, A. S. (1988). Fatigue strength of prestressed concrete girder bridges. *Canadian Journal of Civil Engineering*, **15** (2), 199–205.

[9] Higgins, C., Farrow III, W., Nicholas, B., and Potisuk, T. (2006). High-cycle fatigue of diagonally cracked reinforced concrete bridge girders: Field tests. *J. Bridge Eng. 11, SPECIAL ISSUE: Methods of Monitoring and Evaluating Structural Performance*, 699–706.

[10] Wood, S. L., Hagenberger, M. J., Heller, B. E., and Wagener, P. J. (2007). Evaluation of serviceability requirements for load rating prestressed concrete bridges. Research Report FHWA/TX-07/0-1895-1. Center for Transportation Research Bureau of engineering Research, The University of Texas at Austin.

[11] Hanson, J. M., Hulsbos, C. L., and VanHorn, D. A. (1970). Fatigue tests on prestressed concrete I-beams. *Journal of the Structural Division*, **96** (11), 2443–2464.

[12] Zia, P., Mirza, J. F., and Riskalla, S. H. (1976). Static and fatigue tests of composite T-beams containing prestressed concrete tension elements. *PCI Journal*, **21** (6), 77–93.

[13] Harajli, M. H., and Naaman, A. E. (1985). Static and fatigue tests on partially prestressed beams. *Journal of Structural Engineering*, **111** (7), 1602–1618.

[14] Shahawi, M. E., and Batchelor, B. D. (1986). Fatigue of partially prestressed concrete. *Journal of Structural Engineering*, **112** (3), 524–537.

[15] Naaman, A. E., and Founas, M. (1991). Partially prestressed beams under random-amplitude fatigue loading. *Journal of Structural Engineering*, **117** (12), 3742–3761.

[16] Rao, C., and Frantz, G. C. (1995). Test on prestresses concrete bridges beams-fatigue tests of the bridges beams. Research Report JHR 95-245, University of Connecticut Department of Civil Engineering.

[17] Rao, C., and Frantz, G. C. (1996). Fatigue tests of 27-year-old prestressed concrete bridge box beams. *PCI Journal*, **41** (5), 74–83.

[18] Carpinteri, A., Spangnoli, A., and Vantadori, S. (2005). Mechanical damage of ordinary or prestressed reinforced concrete beams under cyclic bending. *Engeneering Fracture Mechanics* **72**, 1313–1328.

[19] Wollmann, G. P., Yates, D. L., Breen, J. E., and Kreger, M.E. (1996). Fretting fatigue in post-tensioned concrete beams. *ACI Structural Journal*, **93** (2), 172–179.

[20] Cordes, H., Hegger, J., and Neuser, J. U. (2000). Untersuchungen zur Reibermüdung bei teilweise vorgespannten Bauteilen. In: Eligehausen, R., Kordina, K., Schießl, P. (ed.). In: Bewehrte Betonbauteile unter Betriebsbedingungen, Weinheim, Wiley-VCH, 322–335.

[21] Empelmann, M., and Remitz, J. (2014). Fatigue behaviour of post-tensioned tendons / Ermüdungsverhalten von Spanngliedern mit nachträglichem Verbund. *Beton- und Stahlbetonbau* **109** (11), 760–770.

[22] LeBeau, K., and Wadia-Fascetti, S. (2010). Predictive and diagnostic load rating model of a prestressed concrete bridge. *J. Bridge Eng. 15, SPECIAL ISSUE: Bridge Inspection and Evaluation*, 399–407.

[23] Orton, S., Kwon, O., and Hazlett, T. (2012). Statistical distribution of bridge resistance using updated material parameters. *J. Bridge Eng.*, **17** (3), 462–469.

[24] Bocchini, P., Saydam, D., and Frangopol, D. (2013). Efficient, accurate, and simple Markov chain model for the life-cycle analysis of bridge groups. *Structural Safety* **40**, 51–64.

[25] Sobczyk, K., and Spencer, B. F. (1992). *Random fatigue: From data to theory.* Academic Press Limited, London.

[26] Heron, E. A., and Walsh, C. D. (2008). A continuous latent spatial model for crack initiation in bone cement. *Appl. Statist.*, **57**, 25–42.

[27] Doudard, C., Calloch, S., Cugy, P., Galtier, A., and Hild, F. (2005). A probabilistic two-scale model for high-cycle fatigue life predictions. *Fatigue & Fracture of Engineering Materials & Structures* **28**, 279–288.

[28] Yuan, X.-X., Mao, D., and Pandey, M. D. (2009). A Bayesian approach to modeling and predicting pitting flaws in steam generator tubes. *Reliability Engineering and System Safety* **94**, 1838–1847.

[29] EN 1992-1-1 (2004). Design of concrete structures – Part 1–1: General rules and rules for buildings. European Standard.

[30] Comité Euro-International Du Béton (1993). EPF Lausanne CEB-FIB Model Code 1990: Design Code.

[31] Rios Insua, D., Ruggeri, F., and Wiper, M. P. (2012). *Bayesian analysis of stochastic process models.* John Wiley & Sons, United Kingdom.

[32] Yu, J.-W., Tian, G.-L., and Tang, M.-L. (2007). Predictive analyses for nonhomogeneous Poisson processes with power law using Bayesian approach. *Computational Statistics & Data Analysis*, **51**, 4254–4268.

[33] Carlin, B. P., and Louis, T. A. (2009). *Bayesian methods for data analysis.* CRC Press, Boca Raton.

Appendix

Beginning with the function w_k in (7) we abbreviate $\nu = 0.72 \cdot \pi \cdot f_{ctm} \cdot E_p$, think of definition $A_p(n) = A_p \cdot \left(1 - \frac{C_n}{35}\right) = A_p \cdot h(C_n)^{-1}$ and $\Delta\sigma_{pr}(n) = \sigma_{p,max} \cdot \frac{A_p}{A_p(n)} - \sigma_{pm0} = \sigma_{p,max} \cdot h(C_n) - \sigma_{pm0}$ with $h(x) = \frac{1}{1 - \frac{x}{35}}$. It is

$$
\begin{aligned}
w_k&(n) \\
&= \frac{(1 - k_t(n)) \cdot (\Delta\sigma_{pr}(n))^2 \cdot A_p(n)}{0.72 \cdot \pi \cdot f_{ctm} \cdot E_p \cdot \sqrt{A_p(n)}} \\
&= \frac{1}{\nu} \cdot (1 - k_t(n)) \cdot (\Delta\sigma_{pr}(n))^2 \cdot \sqrt{A_p(n)} \\
&= \frac{1}{\nu} \cdot (1 - k_t(n)) \cdot (\sigma_{p,max} \cdot h(C_n) - \sigma_{pm0})^2 \cdot \sqrt{A_p \cdot h(C_n)^{-1}} \\
&= \frac{\sqrt{A_p}}{\nu \cdot \sqrt{h(C_n)}} \cdot (1 - k_t(n)) \cdot (\sigma_{p,max} \cdot h(C_n) - \sigma_{pm0})^2 \\
&= \frac{\sqrt{A_p}}{\nu \cdot \sqrt{h(C_n)}} \cdot (1 - k_{t\to\infty} - (k_{t=0} - k_{t\to\infty}) \cdot e^{n\cdot c}) \cdot \sigma_{p,max}^2 \cdot \left(h(C_n) - \frac{\sigma_{pm0}}{\sigma_{p,max}}\right)^2 \\
&= \frac{\sqrt{A_p} \cdot \sigma_{p,max}^2}{\nu} \cdot ((1 - k_{t\to\infty}) - (k_{t=0} - k_{t\to\infty}) \cdot e^{n\cdot c}) \cdot \frac{1}{\sqrt{h(C_n)}} \cdot \left(h(C_n) - \frac{\sigma_{pm0}}{\sigma_{p,max}}\right)^2 \\
&= (\theta_1 - \theta_2 \cdot \exp(-n \cdot \theta_3)) \cdot \frac{1}{\sqrt{h(C_n)}} (h(C_n) - \theta_4)^2
\end{aligned}
$$

with

- $\theta_1 = \frac{(1 - k_{t\to\infty}) \cdot \sqrt{A_p} \cdot \sigma_{p,max}^2}{0{,}72 \cdot \pi \cdot f_{ctm} \cdot E_p}$,

- $\theta_2 = \frac{(k_{t=0} - k_{t\to\infty}) \cdot \sqrt{A_p} \cdot \sigma_{p,max}^2}{0{,}72 \cdot \pi \cdot f_{ctm} \cdot E_p}$,

- $\theta_3 = -c$,

- $\theta_4 = \frac{\sigma_{pm0}}{\sigma_{p,max}}$.